Green Chemistry

One-Pot Aqueous Synthesis of Ultrathin Trimetallic PdPtCu Nanosheets for the Electrooxidation of Alcohols

Journal:	*Green Chemistry*
Manuscript ID	GC-ART-03-2019-000741
Article Type:	Paper
Date Submitted by the Author:	01-Mar-2019
Complete List of Authors:	Lv, Hao; Nanjing Normal University - Xianlin Campus, Chemistry Sun, Lizhi; Nanjing Normal University, Chemistry and Materials Science Xu, Dongdong; Nanjing Normal University, School of Chemistry and Mateirals Science Suib, Steven; University of Connecticut, U-60, Department of Chemistry Liu, Ben; Nanjing Normal University, Chemistry and Materials Science

Green Chemistry

PAPER

One-pot aqueous synthesis of ultrathin trimetallic PdPtCu nanosheets for the electrooxidation of alcohols

Received 00th January 20xx,
Accepted 00th January 20xx

DOI: 10.1039/x0xx00000x

www.rsc.org/

Hao Lv,[a] Lizhi Sun,[a] Dongdong Xu,[a,*] Steven L. Suib,[b] and Ben Liu[a,*]

Due to synergistically structural and compositional advantages, ultrathin multimetallic nanosheets are widely recognized as the high-efficiency electrocatalysts for alcohol electrooxidation. Despite great efforts, the current synthetic strategies for the preparation of multimetallic nanosheets mainly focus on the reduction of metal precursors in organic solvents or the presence of toxic CO. In this contribution, one-pot aqueous synthesis based on the self-assembly of novel surfactant of docosyltrimethylammonium chloride is employed to produce ultrathin free-standing trimetallic PdPtCu nanosheets under ambient and eco-friendly conditions. No any toxic chemicals (even organic solvent) were employed in the synthesis. The obtained PdPtCu nanosheets are ultrathin with a dendrite-like nanostructure (with an average thickness of ~3.5 nm) and alloyed crystalline feature. The synthetic strategy is also universal for tuning the elemental ratios and compositions of ultrathin multimetallic nanosheets. Due to multiple advantages of unique ultrathin dendrite nanostructures and multimetallic elemental compositions, PdPtCu nanosheets exhibit remarkably enhanced performances in the electrooxidation of alcohols (methanol, ethanol, glycerol and glucose). The one-pot eco-friendly synthetic concept could be expected to build more multimetallic nanostructures with synergic enhancement effect for a range of electrocatalyitc applications.

Introduction

The past two decades have witnessed the significant development for searching sustainable and renewable resources to replace transitional fossil fuels.[1, 2] Direct alcohol fuel cells (DAFCs) have been recognized as one of most important solution,[3-5] because they possess the higher efficiency in energy conversion and better sustainability in the environment. Currently, noble metals of Pd and Pt are still the most efficient anode catalysts for electrocatalyzing alcohol oxidation reactions in DAFCs.[6-10] However, the potential commercialization of the DAFCs is greatly hindered by the high price and poor stability of the nanocatalysts. Nanoalloyed Pd/Pt with secondary metal, such as Au, Ag, Ru, Cu and Zn, has been found to be an attractive route to enhance the utilization efficiency of metal metals and boost the electrocatalytic performance, based on the well-known *d*-band theory.[11-15] Meanwhile, the introduction of more oxophilic metals could efficiently promote the formation of adsorbed OH (OH_{ads}), and thus facilitate the further oxidation/removal of poisoning intermediates on Pd/Pt.[16-19] Such bifunctional effects not only enhance the mass activity, but also improve the long-term stability of the nanocatalysts during the electrocatalysis. The formation of multimetallic nanoalloys with different elemental compositions in one catalyst would further optimize and enhance the electrocatalytic performances (known as a compositionally synergetic enhancement effect).

Apart from the elemental compositions, engineering the nanostructures of noble metal-based catalysts has been recognized as another effective tool to improve the electrocatalytic performances.[20-28] Of various nanostructures available, anisotropic two-dimensional (2D) ultrathin nanosheets with an average thickness less than 5 nm have recently received special attention for electrocatalytic applications, due to the higher exposed and undercoordinated surface sites, and anisotropic nanostructures.[29-37] For example, Zheng et al. found that Pd nanosheets displayed a 2.5-fold enhancement in the electrooxidation of formic acid, compared to commercial Pd NPs.[38] Cheng and his colleagues observed that 2D PdAg nanosheets can retain ~ 50 % activity in ethanol electrooxidation even after 10, 000 cycles.[39] Wang et al. showed that Pt-Cu nanosheets or nanocones exhibited the larger peak current density of ethanol oxidation, almost 22 times that of commercial Pt black and 14 times that of Pt/C.[40, 41] Therefore, we rationally anticipate a highly active and stable electrocatalyst by combining with the above advantages of multimetallic elemental compositions and 2D ultrathin nanostructures. To date, unfortunately, only limited synthetic methods are successfully developed to grow ultrathin noble metal-based nanosheets, principally because anisotropic nanostructure of ultrathin multimetallic nanosheets does not thermodynamically fit to symmetric face-central cubic (fcc) crystalline phases of noble metal nanocrystals. Because toxic CO is universally used as the reducing agent and nanosheet-forming/stabilizing agent during the fabrication of ultrathin nanosheets,[36] concerns about safety and environment should also be seriously resolved. Therefore, a big challenge remains to develop a facile, eco-friendly, and low-cost method to prepare ultrathin

[a] Jiangsu Key Laboratory of New Power Batteries, Jiangsu Collaborative Innovation Center of Biomedical Functional Materials, School of Chemistry and Materials Science, Nanjing Normal University, Nanjing, Jiangsu 210023, China. E-mails: ddxu@njnu.edu.cn (D. Xu); ben.liu@njnu.edu.cn (B. Liu)
[b] Department of Chemistry and Institute of Materials Science, University of Connecticut, Storrs, Connecticut 06269, USA

†Electronic Supplementary Information (ESI) available: additional TEM images, XPS, and electrocatalytic tests. See DOI: 10.1039/x0xx00000x

multimetallic nanosheets, especially through an aqueous synthesis.[42-44]

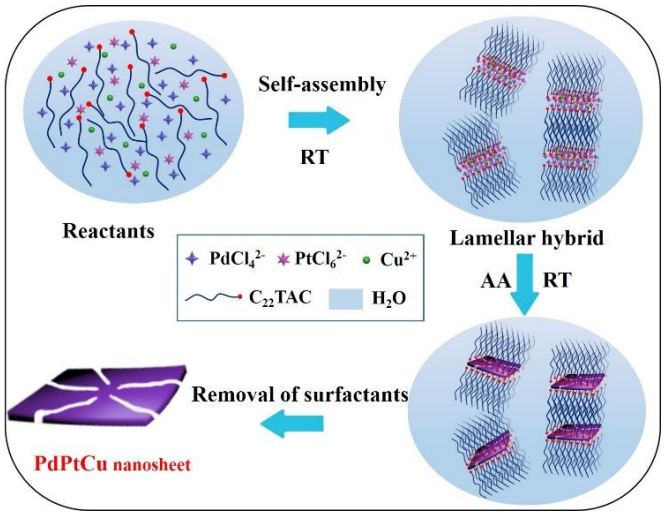

Fig. 1 Schematic illustrating formation of ultrathin free-standing trimetallic PdPtCu nanosheets using the surfactant-directed solution-phase synthesis.

Herein, we developed a one-pot, eco-friendly, reactively prompt synthesis strategy to fabricate ultrathin free-standing trimetallic PdPtCu nanosheets under an aqueous solution, and further investigated their enhanced electrocatalytic performances in alcohol oxidation reactions. Ultrathin PdPtCu nanosheets with a thickness of ~ 3.5 nm and a diameter of ~45 nm were synthesized using docosyltrimethylammonium chloride ($C_{22}TAC$) as the surfactant template, $PdCl_4^{2-}$, $PtCl_6^{4-}$, and Cu^{2+} as metal precursors, and ascorbic acid (AA) as reducing agent at room temperature. No toxic chemicals (even organic solvents) were employed in the synthesis. The introduction of amphiphilic $C_{22}TAC$ with a long-chain alkyl hydrophobic tail, a hydrophilic quaternary ammonium head and a counter ion of Cl^- as the surfactant template is critically important to drive the formation of 2D ultrathin nanosheet structure (see Fig. 1). Meanwhile, elemental ratios and compositions of ultrathin nanosheets were readily tailored by changing initial feed ratios and species of metal precursors. As-resultant ultrathin PdPtCu nanosheets were demonstrated as electrocatalysts for alcohol oxidation reactions, in which remarkably enhanced electrocatalytic performances (activity and stability) were achieved, compared to their counterpart nanocatalysts with bimetallic/monometallic compositions or 0D nanostructures. More importantly, such enhancement is universal in various alcohol electrooxidations (methanol, ethanol, glycerol, and glucose electrooxidation).

Results and Discussion

Synthesis and characterizations of ultrathin PdPtCu nanosheets

In a typical synthesis of ultrathin free-standing PdPtCu nanosheets, H_2PdCl_4, H_2PtCl_6 and $Cu(NO_3)_2$ were added to an aqueous solution containing $C_{22}TAC$ (1.5 mg/mL) under stirring. Subsequently, freshly prepared AA solution was injected, and kept at room temperature for 30 min. As-resultant products were then collected by centrifugation and washed with acetic acid and ethanol/H_2O for three times to remove the surfactants on the surfaces of PdPtCu nanosheets (see experimental section for more details) (Fig. 1).

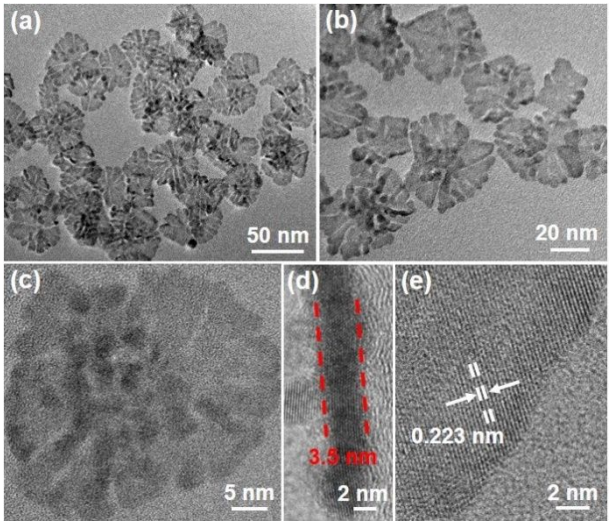

Fig. 2 (a, b) Low-magnification, (c) high-magnification, and (d, e) high-resolution TEM images of ultrathin PdPtCu nanosheets.

Ultrathin free-standing PdPtCu nanosheets were first indicated by low-magnification transition electron microscopy (TEM) images. As shown in Fig. 2a, as-resultant products are ultrathin with a sheet-like nanostructure. The average lateral diameter of PdPtCu nanosheets is 45 nm with a small distribution of 3.5 nm. A clearer observation in Fig. 2b showed that the nanosheets are composed of several radial nanobranches from the same core. Ultrathin dendrite-like nanosheet structures were further observed by a high-magnification TEM image (Fig. 2c). The thickness of ultrathin PdPtCu nanosheets was evaluated to be 3.5 nm with ~ 16 atomic layers (Fig. 2d), when in a perpendicular orientation on carbon supports (see Fig. S1 for low-magnification TEM images†). The high-resolution TEM observation was also shown to unveil the crystalline nature, in which a clear *d*-spacing of 0.223 nm was well-matched to the (111) planes of fcc PdPtCu alloyed nanocrystals (Fig. 2e). The successful formation of ultrathin free-standing nanosheets with dendrite-like nanostructures was also revealed by high-angle annular dark-field scanning TEM (HAADF-STEM) (Fig. 3a).

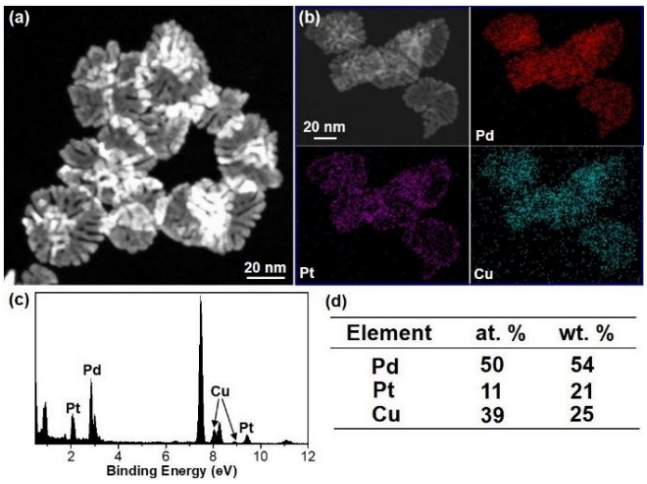

Fig. 3 (a) HAADF-STEM image, (b) elemental mappings, (c) EDX, and (d) corresponding elemental compositions of ultrathin PdPtCu nanosheets.

The elemental compositions and distributions of ultrathin PdPtCu nanosheets were further revealed by STEM mappings and corresponding energy-dispersive X-ray (EDX) spectroscopy. As shown in Fig. 3b, homogeneously distributed Pd, Pt, and Cu were spatially overlapped throughout the whole nanosheets, definitely suggesting ultrathin PdPtCu nanosheets are solid nanoalloys, rather than phase-separated ones. The co-existence of trimetallic PdPtCu was also indicated by STEM-EDX (Fig. 3c). The compositional ratio of Pd, Pt, and Cu in ultrathin PdPtCu nanosheets was determined to be 54:21:25 (by wt. %) (Fig. 3d), similarly to the results collected from X-ray photoelectron spectra (XPS) survey (57: 17: 26, Fig. S2†) and inductively coupled plasma mass spectrometry (58:22: 20).

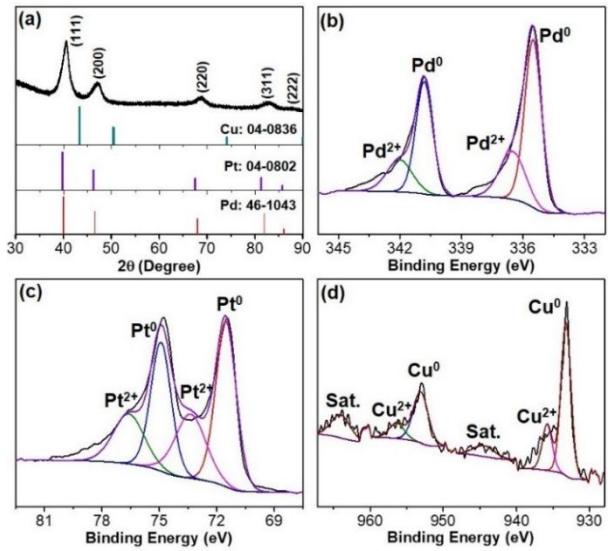

Fig. 4 (a) Wide-angle XRD pattern, (b) high-resolution Pd 3d, (c) Pt 4f, and (d) Cu 2p XPS spectra of ultrathin PdPtCu nanosheets.

The crystalline features and nanoalloyed elemental compositions of ultrathin PdPtCu nanosheets were also indicated by wide-angle X-ray diffraction (XRD) and high-resolution XPS. Five typical XRD peaks located between 30-90° can be assigned to metallic fcc crystalline phases ((111), (200), (220), (311) and (222) planes, respectively) (Fig. 4a). No other peaks ascribed to pure fcc Pd, Pt, or Cu can be observed. Due to the similar fcc crystallographic structure of Pd, Ag, and Cu, wide-angel XRD peaks of metallic alloys strongly depended on the element contents. From XRD patterns, the *d*-spacing of (111) plane was calculated to be 0.222 nm (45.12°) for PdPtCu nanosheets which located in between Pt (0.227 nm) and Cu (0.209 nm), further evidencing the formation of PdPtCu alloys. The high-resolution XPS spectra of Pd 3d, Pt 4f, and Cu 2p were further deconvoluted to unveil the surface elemental states of ultrathin PdPtCu nanosheets. As shown in Fig. 4b, two representative XPS peaks with binding energies of 335.5 and 340.8 eV were assigned to the metallic Pd $3d_{5/2}$ and $3d_{3/2}$, respectively, while the ones at 336.4 and 342.0 eV were attributed to the bivalent Pd^{2+}. Both of these transitions are positively shifted in binding energy relative to pure counterparts, suggesting that the charge transfer between Pd and Pt/Cu modified the electronic structures of Pd in ultrathin PdPtCu nanosheets.[39, 45, 46] The occurrence of the electron transfer in ultrathin PdPtCu nanosheets was also confirmed by slightly shifted XPS peaks of Pt 4f and Cu 2p (Fig. 4c and 4d). The above structural and electronic characterization definitely suggested the successful formation of ultrathin free-standing PdPtCu nanosheets with dendrite-like structures and alloyed crystalline features.

Introduction of C_{22}TAC as the surfactant template is the key to the formation of ultrathin PdPtCu nanosheets. C_{22}TAC highlights three structural features, including the long-chain hydrophobic C_{22} tail, the hydrophilic quaternary ammonium head, and the counter ion of Cl^-.[44,47,48] Among them, i) the hydrophobic C_{22} tail drives the self-assembly into a lamellar mesostructure, ii) the hydrophilic head stabilizes the assembled nanostructure and binds with metal precursors through electrostatic and/or coordination interactions for in-the-plane epitaxial growth of ultrathin nanosheets, and iii) Cl^- assists the formation and stabilization of 2D nanosheets. To further reveal the key factor of C_{22}TAC in the formation of ultrathin PdPtCu nanosheets, more control experiments were also carried out. First, amphiphilic C_{16}TAC with the shorter hydrophobic alkyl tail was used as the surfactant template for the formation of PdPtCu nanoalloys. Mesoporous nanospheres, rather than ultrathin nanosheets, were obtained (Fig. S3a, b†). This can be ascribed to the changed packing parameter (*g* value) of C_{16}TAC that favors self-assembly into hexagonal mesophases. Second, Br^- was used as the counter ion (docosyltrimethylammonium bromide (C_{22}TAB)) for the synthesis. In comparison to Cl^-, Br^- possesses a preferential chemisorption on (110) and (100) planes of Pd, and thus facilitates the growth along specific exposed crystalline planes into the thicker dendrite-like nanoplates (~7-10 nm) (Fig. S3c, d†). Lastly, toxic CO has also been investigated as the reducing agent for driving the reduction of metal precursors. Ultrathin nanosheets were synthesized under the same synthetic conditions (Fig. S3e, f†), further suggesting the importance of C_{22}TAC for fabricating ultrathin multimetallic nanosheets.

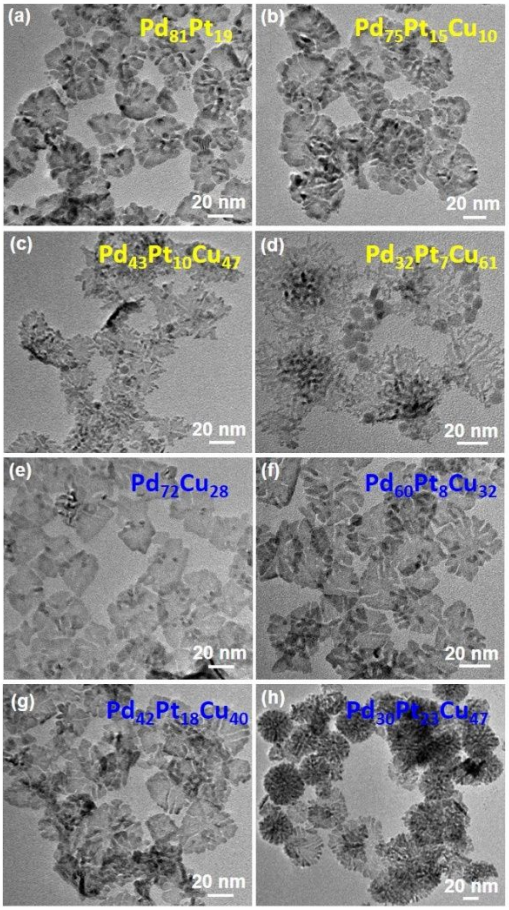

Fig. 5 Multimetallic PdPtCu nanostructures synthesized by changing initial feed ratios of (a-d) Cu and (e-h) Pt.

The elemental ratios of multimetallic nanoalloys are compositionally important to their electrocatalytic performances. In the current work, compositional ratios of PdPtCu nanoalloys were also investigated on their final nanostructures (Fig. 5). We first studied the effect of Cu, and found that perfect ultrathin dendrite-like nanosheets were obtained in Cu content < 25 wt. % (Fig. 5a, b). The higher Cu ratio in PdPtCu nanoalloys (> 47 wt. %) gave rise to more fractal branches of PdPtCu nanosheets (Fig. 5c), in which smaller nanoparticles gradually appeared when Cu content is higher than 61 % (Fig. 5d). Similarly, ultrathin free-standing nanosheets can be synthesized when Pt content is lower than 21 wt. % (Fig. 5e-g). However, the higher Pt content in trimetallic PdPtCu nanoalloys (23 wt. %) may change the self-assembled behavior of the surfactant, and cause the formation of mesoporous nanoparticles (Fig. 5h). The slower crystalline nucleation rate of Pt and Cu (compared to Pd) may suppress the lamellar nanostructures from C_{22}TAC and results in the formation of thermodynamically more stable nanoparticles. These results obviously revealed good controllability in the composition of ultrathin multimetallic PdPtCu nanosheets.

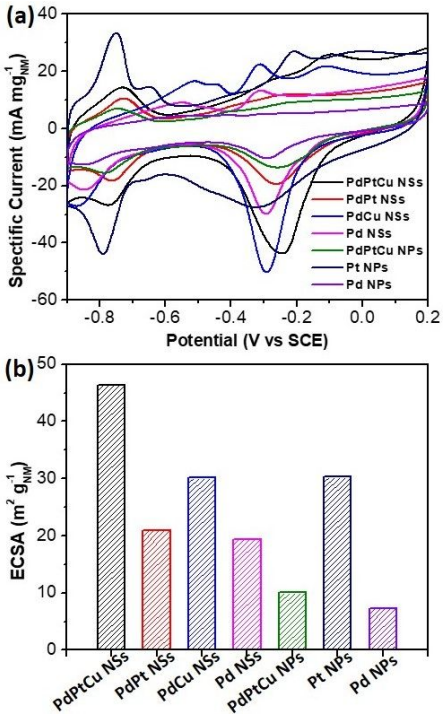

Fig. 6 (a) CV curves and (b) corresponding ECSAs of trimetallic PdPtCu nanosheets (NSs), bimetallic PdPt and PdCu nanosheets, monometallic Pd nanosheets, PdPtCu nanoparticles (NPs), and commercial Pt and Pd nanoparticles obtained in 1.0 M KOH at 50 mV s^{-1}.

Electrocatalytic performance

Ultrathin PdPtCu nanosheets have multiple advantages, including unique ultrathin dendrite-like nanostructures and multimetallic elemental compositions, both of which enhance the utilization efficiency of noble metals and benefit enhanced electrocatalytic performance towards alcohol oxidation reactions. On the one hand, ultrathin nanosheets would expose more electrocatalytic active sites and facilitate electron/mass transfer during the electrocatalysis, compared to their 0D nanoparticle counterparts. Meanwhile, anisotropic nanostructures would also suppress the Ostwald ripening of nanocrystals, strengthening the contraction between nanocatalysts and carbon/electrode, and thus improving their self-stability. On the other hand, trimetallic nanoalloyed compositions render the nanocatalysts with a bifunctional effect. More oxophilic metals of Cu alloyed with Pd/Pt promote the adsorption of OH (Cu-OH_{ads}) and facilitate the direct reaction between Pd/Pt-CO_{ads} and Cu-OH_{ads}. This kinetically accelerates the further oxidation/removal of the intermediates during the electrocatalysis, and enhances their electrocatalytic performances. To reveal the merit of the ultrathin nanosheet structure, 0D PdPtCu nanoparticles which were synthesized in the absence of the surfactant (see TEM images in Fig. S4a, b†) were tested. Similarly, to highlight the advantages of multimetallic compositions, bimetallic PdCu and PdPt nanosheets (Fig. 5a, e), and monometallic Pd nanosheets (see TEM in Fig. S4c, d†) were studied. In addition, commercial Pt and Pd nanoparticles were also investigated for standard comparisons.

Structural and compositional advantages of ultrathin PdPtCu nanosheets were first revealed by CV and corresponding electrocatalytic active surface area (ECSA). Fig. 6a displayed the CVs of PdPtCu nanosheets and their counterparts collected in N_2-saturated 1.0 M KOH (50 mV s^{-1}). Clearly, the reduction peaks (from PdO/PtO to Pd/Pt) located in the range of -0.5 V and 0 V (vs SCE) appeared during the negative scans, indicating the potential of the nanocatalysts for electrocatalyzing alcohol oxidation reactions.[49] Amongst them, the lowest reduction potential and largest area were seen for ultrathin PdPtCu nanosheets, compared to other nanocatalysts, indicating more electrocatalytic active sites and easier reduction of PdO/PtO to Pd/Pt. We further estimated the ECSAs by fully considering the elemental compositions of noble metals (Pd and Pt) based on the Coulombic charges for PdO/PtO reduction.[39, 49, 50] As expected, ultrathin PdPtCu nanosheets exhibited the largest ECSA of 46.3 m^2 g$_{NM}^{-1}$ (Fig. 6b). In contrast, the ECSAs of bimetallic PdPt, PdCu, and monometallic Pd nanosheets are 20.9, 30.1 and 19.4 m^2 g$_{NM}^{-1}$, respectively. Similarly, a smaller ECSA of 10.0 m^2 g$_{NM}^{-1}$ was seen for trimetallic PdPtCu nanoparticles.

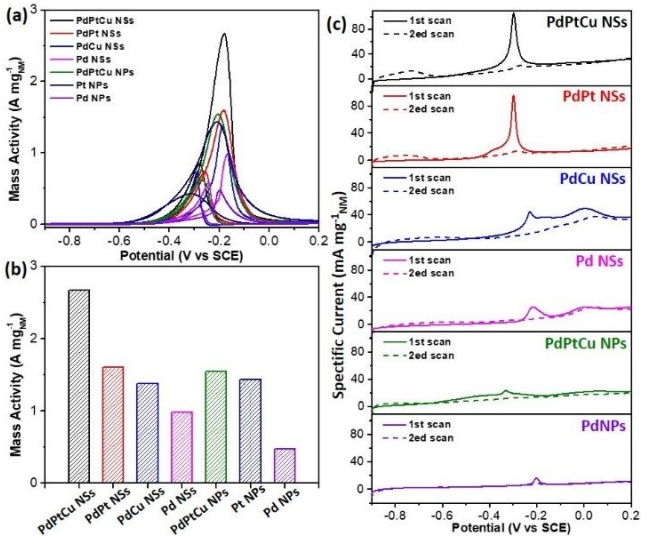

Fig. 7 (a) CV curves and (b) normalized mass activities of trimetallic PdPtCu nanosheets, bimetallic PdPt and PdCu nanosheets, monometallic Pd nanosheets, PdPtCu nanoparticles, and commercial Pt and Pd nanoparticles obtained in 1.0 M KOH and 1.0 M methanol at 50 mV s^{-1}. (c) CO stripping voltammograms collected in 1.0 M KOH at a scan rate of 50 mV s^{-1}.

The enhanced electrocatalytic activity of ultrathin PdPtCu nanosheets was first investigated in methanol oxidation reaction. As shown in Fig. 7a, the CVs of all the nanocatalysts in 1.0 M KOH and 1.0 M methanol are totally different than those obtained in 1.0 M KOH. Two characteristic peaks were seen, indicating the occurrence of methanol electrooxidation. Notably, electrocatalytic activity of methanol oxidation reaction is strongly related to the nanostructures and compositions of the nanocatalysts. Mass activities of all the nanocatalysts were further normalized to their peak currents (Fig. 7b). Remarkably, ultrathin PdPtCu nanosheets exhibited superior electrocatalytic activity with a mass activity of 2.67 A mg_{NM}^{-1}, which is 1.7, 1.9, 2.1, and 1.7 fold higher than that of PdPt nanosheets (1.59 A mg_{NM}^{-1}), PdCu nanosheets (1.38 A mg_{NM}^{-1}), Pd nanosheets (0.98 A mg_{NM}^{-1}), and 0D PdPtCu nanoparticles (1.54 A mg_{NM}^{-1}), respectively. There results also highlighted synergistically structural and compositional merits of ultrathin PdPtCu nanosheets in methanol electrooxidation (Table S1†). For comparison, the mass activities of commercial Pd and Pt nanoparticles are only 1.43 and 0.47 A mg_{NM}^{-1}, respectively. Enhanced electrocatalytic performances of ultrathin PdPtCu nanosheets were also confirmed by CO anti-poisoning experiments (Fig. 7c). Apparently, ultrathin PdPtCu nanosheets exhibited the lowest onset potential and the largest oxidation active area, indicating better ability for further oxidation/removal of the intermediates during the electrocatalysis.[16, 49]

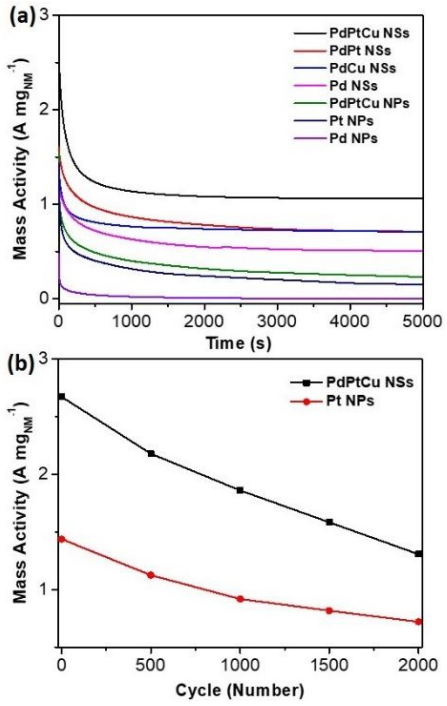

Fig. 8 (a) i-t chronoamperometry curves of trimetallic PdPtCu nanosheets, bimetallic PdPt and PdCu nanosheets, monometallic Pd nanosheets, PdPtCu nanoparticles, and commercial Pt and Pd nanoparticles at the fixed potential of -0.2 V. (b) The long-term cycling stability curves of ultrathin PdPtCu nanosheets and commercial Pt nanoparticles.

We further studied the stability of ultrathin PdPtCu nanosheets, since this is another severe challenge for the development of the electrocatalysts towards alcohol oxidation reactions. We expected that synergistically structural and compositional advantages of ultrathin PdPtCu nanosheets can also improve their electrocatalytic stability. First, the electrocatalytic stabilities of the nanocatalysts were studied by current-time (i-t) chronoamperometry measurements at a fixed potential of -0.2 V (Fig. 8a). A fast activity loss was observed for all the nanocatalysts, due to the dissolution and partial poisoning. However, the retained activity is obviously different. After the electrocatalysis for 5,000 s, ultrathin PdPtCu nanosheets still retained a mass activity of 1.09 A mg_{NM}^{-1} (40.5 %). In contrast, the lower retained mass activity is 0.72 A mg_{NM}^{-1} for PdPt nanosheets, 0.72 A mg_{NM}^{-1} for PdCu nanosheets, 0.51 A mg_{NM}^{-1} for Pd nanosheets, and 0.23 A mg_{NM}^{-1} for PdPtCu nanoparticles. Second, the cycling stability of ultrathin PdPtCu nanosheets was investigated by successive CV scans (Fig. 8b). Similarly, mass activity of ultrathin PdPtCu nanosheets declined to 1.31 A mg_{NM}^{-1} after 2,000 cycles (Fig. S5†), which is 1.7 fold higher than that of Pt NPs (0.72 A mg_{NM}^{-1}). These results further suggest that ultrathin PdPtCu nanosheets intrinsically possessed better electrocatalytic stability. Additionally, we also compared the methanol electrocatalytic performance of PdPtCu nanosheets reduced by AA and CO. As shown in Fig. S6, low mass activity and electrocatalytic stability were found for PdPtCu nanosheets by CO, which may be caused by the relatively irregular nanosheets structures.

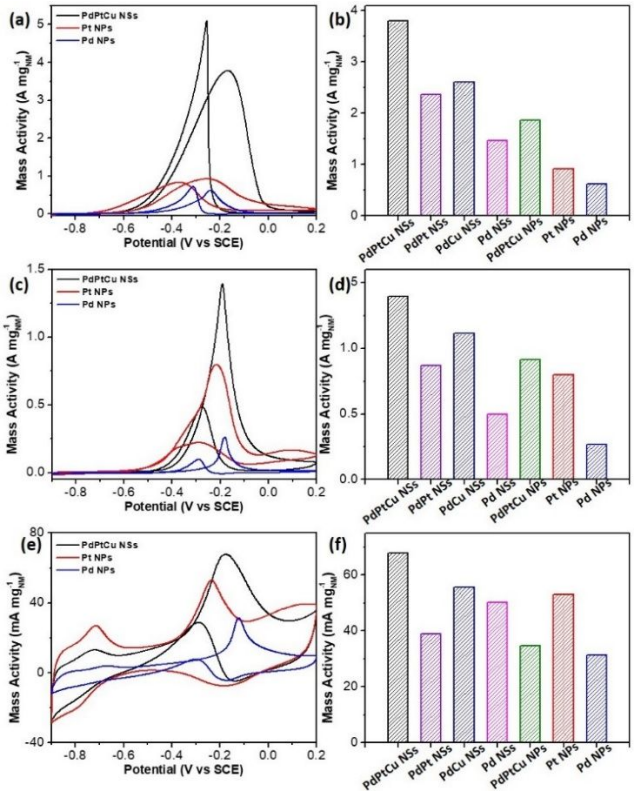

Fig. 9 CV curves of ultrathin PdPtCu nanosheets, commercial Pt and Pd nanoparticles for (a) ethanol, (c) glycerol and (e) glucose electrooxidation. Normalized mass activities of trimetallic PdPtCu nanosheets, bimetallic PdPt and PdCu nanosheets, monometallic Pd nanosheets, PdPtCu nanoparticles, and commercial Pt and Pd nanoparticles for (b) ethanol, (d) glycerol and (f) glucose electrooxidation.

Ultrathin PdPtCu nanosheets are electrocatalytically active not only in methanol oxidation, but also in other alcohol oxidations. As shown in Fig. 9, ultrathin PdPtCu nanosheets were remarkably active in ethanol, glycerol and glucose electrooxidation, with respect to its

bimetallic/monometallic or 0D counterparts and commercial Pt and Pd nanoparticles (see all CVs in Fig. S7-9†). For example, mass activity of ultrathin PdPtCu nanosheets in ethanol electrooxidation is 3.79 A mg_{NM}^{-1}, which is 1.5-2.5 fold higher than its counterparts and 4-6 fold higher than Pt and Pd nanoparticles (Fig. 9b). These results implied that synergistic structural and compositional advantages of ultrathin PdPtCu nanosheets again contributed to enhanced electrocatalytic alcohol oxidation reactions.

Conclusion

In summary, ultrathin free-standing trimetallic PdPtCu nanosheets with dendrite-like nanostructures and tailorable elemental compositions were successfully synthesized through a one-pot, eco-friendly, aqueous synthetic method. Control experiments implied that rationally designed C_{22}TAC with the long-chain alkyl tails and counter ions of Cl^- as the surfactant template are critical for nanoconfining the in-the-plane growth of ultrathin PdPtCu nanosheets. As-resultant nanosheets have multiple advantages, including structurally ultrathin (3.5 nm) and dendrite nanosheets, and compositionally multimetallic elements, and thus synergistically enhanced electrocatalytic activity and stability in alcohol oxidation reactions. Our synthetic strategy is powerful and can readily provide a new avenue to synthesize other multimetallic ultrathin nanosheets (for example, PdAgCu in Fig. S10†) with synergistic enhancement effects for various electrocatalytic applications.

Experimental Section

Synthesis of PdPtCu nanosheets

Ultrathin PdPtCu nanosheets were synthesized by a solution-phase route using C_{22}TAC as surfactant, H_2PdCl_4, H_2PtCl_6 and $Cu(NO_3)_2$ as metal precursors and AA as reducing agent. Typically, 15 mg of C_{22}TAC was totally dissolved in 10 mL of H_2O at 50 °C, followed by the addition of 0.2 mL of NaOH (0.1 M) when cooling down to room temperature. Then, 0.5 mL of 10 mM H_2PdCl_4, 0.15 mL of 10 mM H_2PtCl_6 and 0.15 mL of 10 mM $Cu(NO_3)_2$ were added, and further incubated at 25 °C for 20 min. Subsequently, 1.0 mL of freshly prepared ascorbic acid (AA, 0.3 M) was injected into the above solution with gentle shaking, followed by a color change from yellow to black. After being undisturbed for 30 min, ultrathin PdPtCu nanosheets were collected by centrifugation and were washed with acetic acid and ethanol/H_2O for three times. Similarly, PdPtCu nanostructures with different compositional ratios were synthesized by easily changing initial feed ratios. PdPt, PdCu, and PdAgCu nanosheets were obtained following similar procedures. PdPtCu nanoparticles were synthesized with the same reactants except in the absence of C_{22}TAC.

Electrochemical measurements

Electrocatalytic tests were performed on the CHI 660E electrochemical analyzer at 25 °C. A three-electrode system was used for all electrochemical tests, in which glassy carbon electrodes (GCE, 0.07065 cm^2), carbon rods, and saturated calomel electrodes were used as the working electrode, the counter electrode, and the reference electrode, respectively. For the ink of the nanocatalysts, 1 mg of nanocatalysts, 4 mg of Vulcan XC-72 carbon, and 50 µL of Nafion solution (5 wt% in alcohol and H_2O) were mixed into 1.5 mL of ethanol and 0.5 mL of H_2O. 6 µL of the above-prepared ink solution was directly dropped on the GCE electrode and dried at 40 °C before testing. Cyclic voltammograms (CVs) were successively scanned until the stabilized curves were obtained for further removal of the surfactant in N_2-saturated 1.0 M KOH. Mass activities of the nanocatalysts for methanol electrooxidation were collected by scanning CVs in 1.0 M KOH and 1.0 M methanol with a scan rate of 50 mV s^{-1}. In contrast, we evaluated ethanol electrooxidation in 1.0 M KOH and 1.0 M methanol, glycerol electrooxidation in 1.0 M KOH and 0.1 M glycerol, and glucose electrooxidation in 0.1 M NaOH and 0.01 M glucose. In the present study, all the results (electrochemical active surface area and mass activity) were normalized to the amount of noble metals (Pd and Pt).

Structural and compositional characterizations

TEM was carried out using a JEOL 2010 with an accelerating voltage of 200 kV. HAADF-STEM and corresponding line scans were performed on an FEI Talos F200X instrument at an accelerating voltage of 200 kV. XRD patterns were collected on powder samples using a D/max 2500 VL/PC diffractometer equipped with graphite-monochromatized Cu Kα radiation (30-90°). XPS were performed on a scanning X-ray microprobe (Thermo ESCALAB 250Xi) that uses Al Kα radiation. ICP-MS was recorded on a NexION 350D.

Acknowledgements

BL acknowledges the financial support from Jiangsu Specially Appointed Professor Plan, Natural Science Foundation of Jiangsu Province (No. BK20180723). DDX thanks the support from National Natural Science Foundation of China (No. 21501095). SLS thanks the US Department of Energy for the support of this work under grant DE-FG02-86ER13622.A000. This work is also supported by Priority Academic Program Development of Jiangsu Higher Education Institutions, National and Local Joint Engineering Research Center of Biomedical Functional Materials.

Conflict of interest

The authors declare no conflict of interest.

Notes and references

1 A. K. Mohanty, M. Misra and L. Drzal, *J. Polym. Environ.*, 2002, **10**, 19-26.
2 S. Chu and A. Majumdar, *Nature*, 2012, **488**, 294.
3 E. Antolini and E. Gonzalez, *J. Power Sources*, 2010, **195**, 3431-3450.
4 M. Kamarudin, S. K. Kamarudin, M. Masdar and W. R. W. Daud, *Int. J. Hydrogen Energy*, 2013, **38**, 9438-9453.
5 C. Lamy, A. Lima, V. LeRhun, F. Delime, C. Coutanceau and J.-M. Léger, *J. Power Sources*, 2002, **105**, 283-296.
6 C. Bianchini and P. K. Shen, *Chem. Rev.*, 2009, **109**, 4183-4206.
7 A. Chen and C. Ostrom, *Chem. Rev.*, 2015, **115**, 11199-12044.
8 W. Zhou, Z. Zhou, S. Song, W. Li, G. Sun, P. Tsiakaras and Q. Xin, *Appl. Catal. B-Environ.*, 2003, **46**, 273-285.
9 L. Zhang, Q. Chang, H. Chen and M. Shao, *Nano Energy*, 2016, **29**, 198-219.
10 Y. Xu and B. Zhang, *Chem. Soc. Rev.*, 2014, **43**, 2439-2450.
11 M. Luo, Y. Sun, L. Wang and S. Guo, *Adv. Energy Mater.*, 2017, **7**, 1602073.
12 H.-l. Liu, F. Nosheen and X. Wang, *Chem. Soc. Rev.*, 2015, **44**, 3056-3078.
13 Z. W. Seh, J. Kibsgaard, C. F. Dickens, I. Chorkendorff, J. K. Nørskov and T. F. Jaramillo, *Science*, 2017, **355**, eaad4998.
14 C. Chen, Y. Kang, Z. Huo, Z. Zhu, W. Huang, H. L. Xin, J. D. Snyder, D. Li, J. A. Herron and M. Mavrikakis, *Science*, 2014, **343**, 1339-1343.

15 V. R. Stamenkovic, B. S. Mun, M. Arenz, K. J. Mayrhofer, C. A. Lucas, G. Wang, P. N. Ross and N. M. Markovic, *Nat. Mater.*, 2007, **6**, 241.
16 X. L. Chen, J. C. Li, Y. Z. Huang, J. P. Wei, D. Sun and N. F. Zheng, *Biomater. Sci.*, 2017, **5**, 2448-2455.
17 W. Huang, X. Kang, C. Xu, J. Zhou, J. Deng, Y. Li and S. Cheng, *Adv. Mater.*, 2018, **30**, 1706962.
18 X. Zhao, M. Yin, L. Ma, L. Liang, C. Liu, J. Liao, T. Lu and W. Xing, *Energy Environ. Sci.*, 2011, **4**, 2736-2753.
19 A. Mahmood, N. Xie, M. A. Ud Din, F. Saleem, H. Lin and X. Wang, *Chem. Sci.*, 2017, **8**, 4292-4298.
20 H. Xu, B. Yan, S. Li, J. Wang, C. Wang, J. Guo and Y. Du, *Chem. Eng. J.*, 2018, **334**, 2638-2646.
21 S. Z. Butler, S. M. Hollen, L. Cao, Y. Cui, J. A. Gupta, H. R. Gutierrez, T. F. Heinz, S. S. Hong, J. Huang and A. F. Ismach, *ACS nano*, 2013, **7**, 2898-2926.
22 A. Gupta, T. Sakthivel and S. Seal, *Prog. Mater Sci.*, 2015.
23 P. K. Jain, X. Huang, I. H. El-Sayed and M. A. El-Sayed, *Acc. Chem. Res.*, 2008, **41**, 1578-1586.
24 H. Xu, B. Yan, S. Li, J. Wang, P. Song, C. Wang, J. Guo and Y. Du, *J. Power Sources*, 2018, **384**, 42-47.
25 H. H. Li, S. Y. Ma, Q. Q. Fu, X. J. Liu, L. Wu and S. H. Yu, *J. Am. Chem. Soc.*, 2015, **137**, 7862-7868.
26 B. Lim and Y. Xia, *Angew. Chem. Int. Ed. Engl.*, 2011, **50**, 76-85.
27 C. Zhu, D. Du, A. Eychmuller and Y. Lin, *Chem. Rev.*, 2015, **115**, 8896-8943.
28 Y. Yamauchi, A. Tonegawa, M. Komatsu, H. Wang, L. Wang, Y. Nemoto, N. Suzuki and K. Kuroda, *J. Am. Chem. Soc.*, 2012, **134**, 5100-5109.
29 M. A. Z. G. Sial, M. A. U. Din and X. Wang, *Chem. Soc. Rev.*, 2018, **47**, 6175-6200.
30 T. Ling, J. J. Wang, H. Zhang, S. T. Song, Y. Z. Zhou, J. Zhao and X. W. Du, *Adv. Mater.*, 2015, **27**, 5396-5402.
31 S. Hu and X. Wang, *Chem. Soc. Rev.*, 2013, **42**, 5577-5594.
32 H. L. Qin, D. Wang, Z. L. Huang, D. M. Wu, Z. C. Zeng, B. Ren, K. Xu and J. Jin, *J. Am. Chem. Soc.*, 2013, **135**, 12544-12547.
33 H. Duan, N. Yan, R. Yu, C. R. Chang, G. Zhou, H. S. Hu, H. Rong, Z. Niu, J. Mao, H. Asakura, T. Tanaka, P. J. Dyson, J. Li and Y. Li, *Nat. Commun.*, 2014, **5**, 3093.
34 J. Ge, P. Wei, G. Wu, Y. Liu, T. Yuan, Z. Li, Y. Qu, Y. Wu, H. Li, Z. Zhuang, X. Hong and Y. Li, *Angew. Chem. Int. Ed. Engl.*, 2018, **57**, 3435-3438.
35 L. Dai, Q. Qin, P. Wang, X. Zhao, C. Hu, P. Liu, R. Qin, M. Chen, D. Ou and C. Xu, *Sci. Adv.*, 2017, **3**, e1701069.
36 Y. Chen, Z. Fan, Z. Zhang, W. Niu, C. Li, N. Yang, B. Chen and H. Zhang, *Chem. Rev.*, 2018, **118**, 6409-6455.
37 W. Zhu, L. Zhang, P. Yang, C. Hu, Z. Luo, X. Chang, Z. J. Zhao and J. Gong, *Angew. Chem. Int. Ed.*, 2018, **57**, 11544-11548.
38 X. Huang, S. Tang, X. Mu, Y. Dai, G. Chen, Z. Zhou, F. Ruan, Z. Yang and N. Zheng, *Nat. Nanotechnol.*, 2011, **6**, 28-32.
39 W. Huang, X. Kang, C. Xu, J. Zhou, J. Deng, Y. Li and S. Cheng, *Adv. Mater.*, 2018, **30**, 1706962.
40 F. Saleem, B. Xu, B. Ni, H. Liu, F. Nosheen, H. Li and X. Wang, *Adv. Mater.*, 2015, **27**, 2013-2018.
41 F. Saleem, Z. Zhang, B. Xu, X. Xu, P. He and X. Wang, *J. Am. Chem. Soc.*, 2013, **135**, 18304-18307.
42 H. Lv, A. Lopes, D. Xu and B. Liu, *ACS Cent. Sci.*, 2018, **4**, 1412-1419.
43 H. Lv, X. Chen, D. Xu, Y. Hu, H. Zheng, S. L. Suib and B. Liu, *Appl. Catal. B-Environ.*, 2018, **238**, 525-532.
44 D. Xu, X. Liu, H. Lv, Y. Liu, S. Zhao, M. Han, J. Bao, J. He and B. Liu, *Chem. Sci.*, 2018, **9**, 4451-4455.
45 S. Fu, C. Zhu, D. Du and Y. Lin, *ACS Appl. Mater. Interfaces*, 2015, **7**, 13842-13848.
46 S. H. Han, H. M. Liu, P. Chen, J. X. Jiang and Y. Chen, *Adv. Energy Mater.*, 2018, 1801326.
47 D. Xu, H. Lv, H. Jin, Y. Liu, Y. Ma, M. Han, J. Bao and B. Liu, *J. Phys. Chem. Lett.*, 2019, **10**, 663-671.
48 D. Xu, Y. Liu, S. Zhao, Y. Lu, M. Han and J. Bao, *Chem. Commun.*, 2017, **53**, 1642-1645.
49 J. W. Hong, Y. Kim, D. H. Wi, S. Lee, S. U. Lee, Y. W. Lee, S. I. Choi and S. W. Han, *Angew. Chem. Int. Ed.*, 2016, **55**, 2753-2758.
50 Y. Yang, L. Jin, B. Liu, P. Kerns and J. He, *Electrochim. Acta*, 2018, **269**, 441-451.

Ultrathin PdPtCu nanosheets are prepared by a facile, eco-friendly, and low-cost synthetic method and exhibited remarkably enhanced performances towards various electrocatalytic alcohol oxidations, due to synergistically structural and compositional advantages.